Seismic Fragility Analysis of RC Continuous Girder Bridges Using Artificial Neural Network

Alireza Yazdankhah [a], Araliya Mosleh [b,*], Fatemeh P.Manjily [a], Mehran S.Razzaghi [a]

[a]*Department of Civil Engineering, Qazvin Branch, Islamic Azad University, Qazvin, Iran*

[b] *Post-Doctoral research, CONSTRUCT – LESE, Faculty of Engineering (FEUP), University of Porto, Portugal*

Abstract

This research aims to develop seismic fragility curves for small- and medium-sized concrete bridges. Fragility curves were generated as a function of the probability of reaching or exceeding a specific limit state in terms of the peak ground acceleration (PGA) and acceleration spectral intensity (ASI). To this end, a hybrid dataset of the seismic performances of bridges was prepared by combining the results of numerical analyses and neural predictions. Three-dimensional finite-element models for 1032 bridge-earthquake cases were created, considering the nonlinear behavior of critical bridge components. In addition, multilayer perceptron (MLP) neural networks were employed to simulate artificial earthquake-bridge performance scenarios. The yield stress of reinforcing bars (Fy), the bridge height (H) as well as PGA and ASI, were considered as the input vectors of the artificial neural networks (ANN). The results of this study revealed that MLP neural networks are capable of simulating the seismic performances of bridges appropriately. It was also shown that providing a hybrid dataset of numerical results and neural predictions could lead to the fragility curves of higher correlation coefficients. The results also presented that the PGA-based fragility curves had better correlation coefficients comparing to ASI-based ones.

Keywords: Seismic performance; Artificial neural network; Concrete bridge; Fragility curves

1.Introduction

Bridges are essential components of transportation networks all around the world. According to their critical role in transportation, bridges should be serviceable during and after natural disasters such as earthquakes. In other words, in addition to direct physical loss, bridge damage may cause drastic indirect impacts due to traffic disruption. Note in this regard that relief operations after catastrophic natural disasters can considerably suffer from traffic jam. However, recent seismic events, such as the Kobe earthquake of 1995 in Japan, the Northridge earthquake of 1994 in the USA, the Bam and Varzaghan seismic events of Iran in 2003 and 2011 respectively, caused different levels of damages to various bridges [1-4]. Hence, the seismic vulnerability of existing bridges has attracted several researchers to investigate the seismic performances of different types of bridges [5-10].

Several methods are available for evaluating the seismic performance of a particular structure. Employing fragility functions is a well-known approach to the seismic performance assessment of bridges. The fragility curves are functions that explain the probability of reaching or exceeding a specific damage state in terms of the severity of ground motion [11-14]. The idea of utilizing fragility curves was firstly developed by Whitman et al. [15] and implemented in structures by Veneziano et al. [16]. In recent decades at least four methods have been developed for deriving fragility functions: judgmental [17, 18], empirical [10, 19, 20], analytical [13, 14, 21-24], and hybrid [25]. All the methods mentioned above have their advantages and limitations. The developments of software and computing systems have led to the development of several analytical fragility functions for bridges during the recent decade.

Analytical seismic fragility curves for bridges can be constructed based on various nonlinear analyses such as pushover, nonlinear response history, and incremental dynamic analysis [22, 26-34]. Nonlinear analyses are time-consuming and require a

considerable amount of computer memory. They may also encounter convergence problems. Meanwhile, to achieve a reliable fragility curve, remarkable numbers of nonlinear analyses are required. Therefore, the development of fragility curves using nonlinear analysis (NA) is expensive. It is computationally time-consuming and sometimes impractical, mainly when complex systems such as bridges are analyzed. Therefore, soft computing techniques such as artificial neural networks (ANN) seem to be proper alternatives due to their ability to reduce the number of analyzes in parametric studies [35]. Artificial Neural Networks (ANN) are biologically inspired mathematical paradigms. They can establish a mapping between input vectors to an output one. Artificial neural networks are experiment-based. Therefore, they can learn through examples and recognize complicated relations among various parameters. Hence, ANN can predict the quantities, which are difficult to be measured in a laboratory or calculated by numerical analysis. Different types of ANNs can be employed for solving a particular problem. The multilayer perceptron (MLP), radial basis function network (RBFN) [36], the probabilistic neural network (PNN) [37], and the learning vector quantization (LVQ) [38], are some of the common types of ANNs [39, 40]. Recently, artificial neural networks have been employed in various Civil Engineering trends, including Earthquake Engineering [41-44], Structural Engineering [40], and Geotechnical Engineering [45, 46]. Although there is a large body of research publication on the construction of

analytical fragility curves for RC bridges, reported literature on the topic of neural network-based fragility analysis of such structures are very limited.

In this research, a nonlinear response history analysis was utilized to develop analytical fragility curves for a group of existing pre-1990 continuous deck RC bridges. In addition, the seismic performance of the bridges was predicted using an artificial neural network trained with analytical data. From response history analysis outputs, 70% of data were randomly used for network training, and the remained 30% were utilized for network testing. After selecting the appropriate architecture and structure for the MLP network, 1032 new data were generated. Finally, a combination of nonlinear response history analysis and neural prediction was used to prepare the required dataset of fragility analysis.

2. Specifications of the Studied Bridges

In this study, six common types of highway bridges were selected. More details regarding the selecting procedure of bridges are provided by [21]. The bridges are of multi-span continuous RC types. It is worth mentioning that all of the selected bridges were designed and constructed before 1990 in Iran. The material properties and structural characteristics of the bridges are presented in Tables 1 and 2 and Fig. 1. The superstructures comprise reinforced concrete slabs supported with concrete girders. All the bridges have RC framed piers of circular cross-sections.

Table 1
Structural properties of selected bridges

Column height (H_{col}) (m)	F_y(bar) Mpa	f'_c(col) Mpa	Longitudinal bar of column	Transverse bar of column	1st natural frequency (s)	Bearing stiffness abutments (kN/mm)	
						K_z	K_v
4-8	300-392	31.5	18Φ25	Φ12@20	0.36-0.73	1077	3.12

Table 2
Specifications of selected bridges

Column height (H_{col}) (m)	Column diameters, (c) (m)	Total bridge length (m)	Number of spans	Total span width, (W) (m)	Column spacing, (d) (m)
4-8	1.0	80	4	22.5	8.64

(a)

(b)

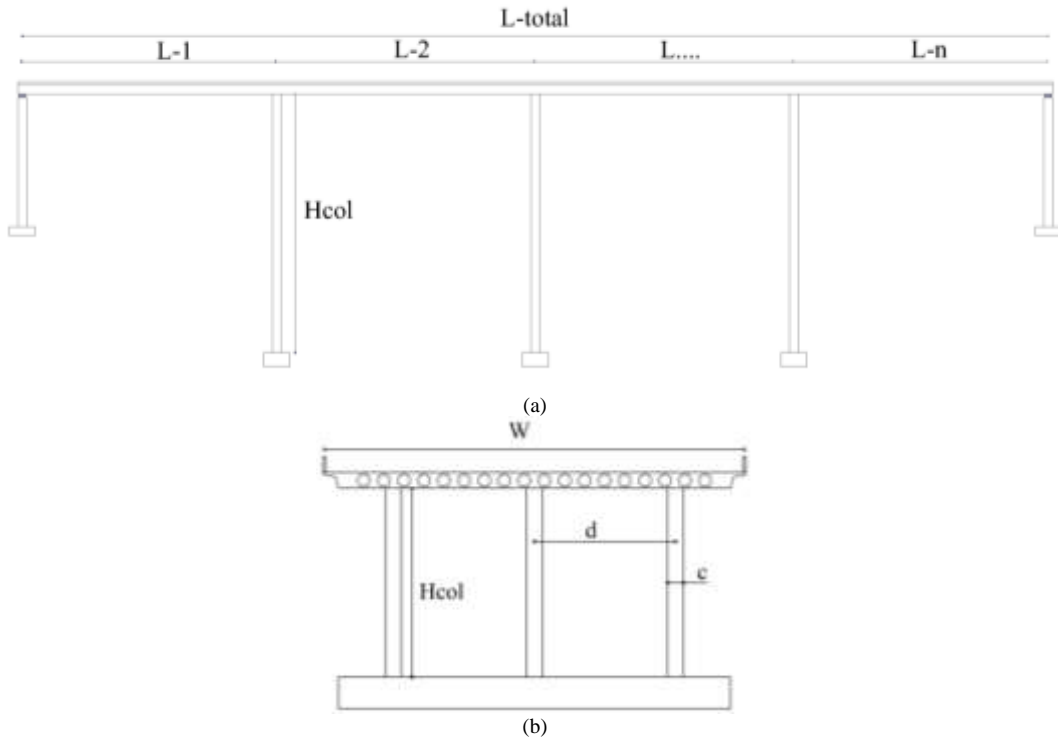Fig 1. Geometry of the bridges (a) Longitudinal direction, (b) Transversal direction

$$\varepsilon_{cc} = 0.002\left(1 + 5\frac{f'_{cc}}{f'_c} - 1\right) \tag{2}$$

3. Nonlinear Response History Analyses

In order to evaluate the seismic performances of the studied bridges, three-dimensional bridge models were implemented with SAP2000 software to conduct nonlinear response history analyses [47].

3.1. Modeling

In this study, frame elements were used to model girders, cap beams and columns. It noteworthy that the frame elements have six degrees of freedom at each node. The following equation was proposed in [48] for the strength parameters of confined concrete.

$$f'_{cc} = f'_c\left(2.254\sqrt{1 + \frac{7.94f'_l}{f'_c}} - \frac{2f'_l}{f'_c} - 1.254\right) \tag{1}$$

where f'_{cc} is the compressive strength of confined concrete, f'_l is the effective lateral compressive strength, and f'_c is the compressive strength of concrete. Also, the maximum compressive strain of concrete ε_{cc} can be obtained from Eq. 2.

The ultimate compressive strain can be obtained from the following equation:

$$\varepsilon_{cu} = 0.004 + \frac{1.4\rho_s f_{yh}\varepsilon_{su}}{f'_{cc}} \tag{3}$$

where ρ_s is the volume fraction of the confined steel, ε_{su} is the steel strain corresponding to the maximum flexural stress, and f_{yh} is the yield strength of the transverse steel. Moreover, ρ_s and f'_l in Eqs. 3 and 1 can be obtained from Eqs. 4 and 5, respectively.

$$\rho_s = \frac{4A_h}{D's} \tag{4}$$

$$f'_l = \frac{1}{2}k_e\rho_s f_{yh} \tag{5}$$

where A_h is the cross-sectional area of the transverse bar, D' is the width of the core of the confined concrete, s is the longitudinal distance of the hoops, and k_e is the confinement ratio. The abutments were modeled by the elastic springs recommended in Caltrans [49] in longitudinal and transversal directions. The analysis of the longitudinal response of the abutments is expressed using a bilinear

approximation from the deformation-force or deformation-nonlinear force relationships [50]. Based on [49], initial stiffness K_i was assumed as 14.35 KN/mm/m. The abutment's initial stiffness can be calculated proportionate to the back-wall height of the abutment using Eq. 6, where h_{abut} and W_{abut} are the height and width of the abutment, respectively.

$$K_{abut} = K_i W_{abut} \left(\frac{h_{abut}}{1.7} \right) \qquad (6)$$

Elastomeric bearings were modeled as springs. The stiffness of such springs were denoted by [51]:

$$K_v = \frac{GA_g}{H_t} \qquad (7)$$

$$K_s = \frac{6GA_g KS^2}{(6GS^2 + KH_t)} \qquad (8)$$

Where K_v and K_s are the vertical and the shear stiffness of the bearings. G is the shear modulus of rubber (considers 1 MPa in this study), A_g is the gross rubber area, and H_t is the total rubber height. K is the rubber bulk modulus and S is the shape factor. Elastic springs were used to model the abutment and backfill soil, in the longitudinal and transversal directions [49]. Abutment longitudinal response analysis could be explained by considering a bilinear approximation of the force–deformation relationship [52]. The bilinear demand, which includes the effective abutment stiffness, is influenced by expansion gaps, and it includes a realistic value for the embankment fill response. Based on force-deflection results from large-scale abutment testing [50, 53, 54] and passive earth pressure, the initial stiffness K_i is considered as 14.35 kN/mm/m based on the Caltrans recommendation [49]. Fig. 2 demonstrates the 3D model of one of the studied bridges with elements details in SAP2000 software [47].
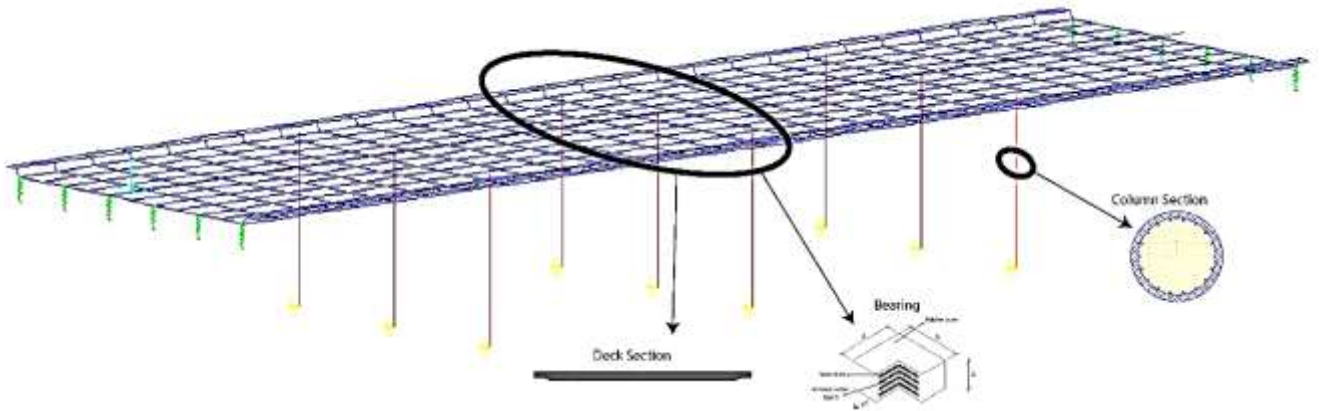

Fig 2. 3D finite element model of 8 m column bridge

P-delta effects were considered in two orthogonal directions. Newmark's beta method was employed to solve dynamic equations. Rayleigh damping coefficients proportional to mass and stiffness were determined by taking into account the first two modal periods. Lumped plastic hinges were modeled at the top and the bottom of columns based on Caltrans recommendation [49, 50]. Fig. 3 demonstrates the hinging mechanism of the 8-m bridge as a sample of the selected bridges for nonlinear response history analysis subjected to Northridge ground motion analysis with PGA= 0.5908g. The figures are related to different steps in the analysis; such as steps 0, 500, 1000, 1500, and 1800. As mentioned before, column elements were modeled with lumped plasticity by defining plastic hinges at both ends of the columns. The side pier was the most critical one subjected to this record.
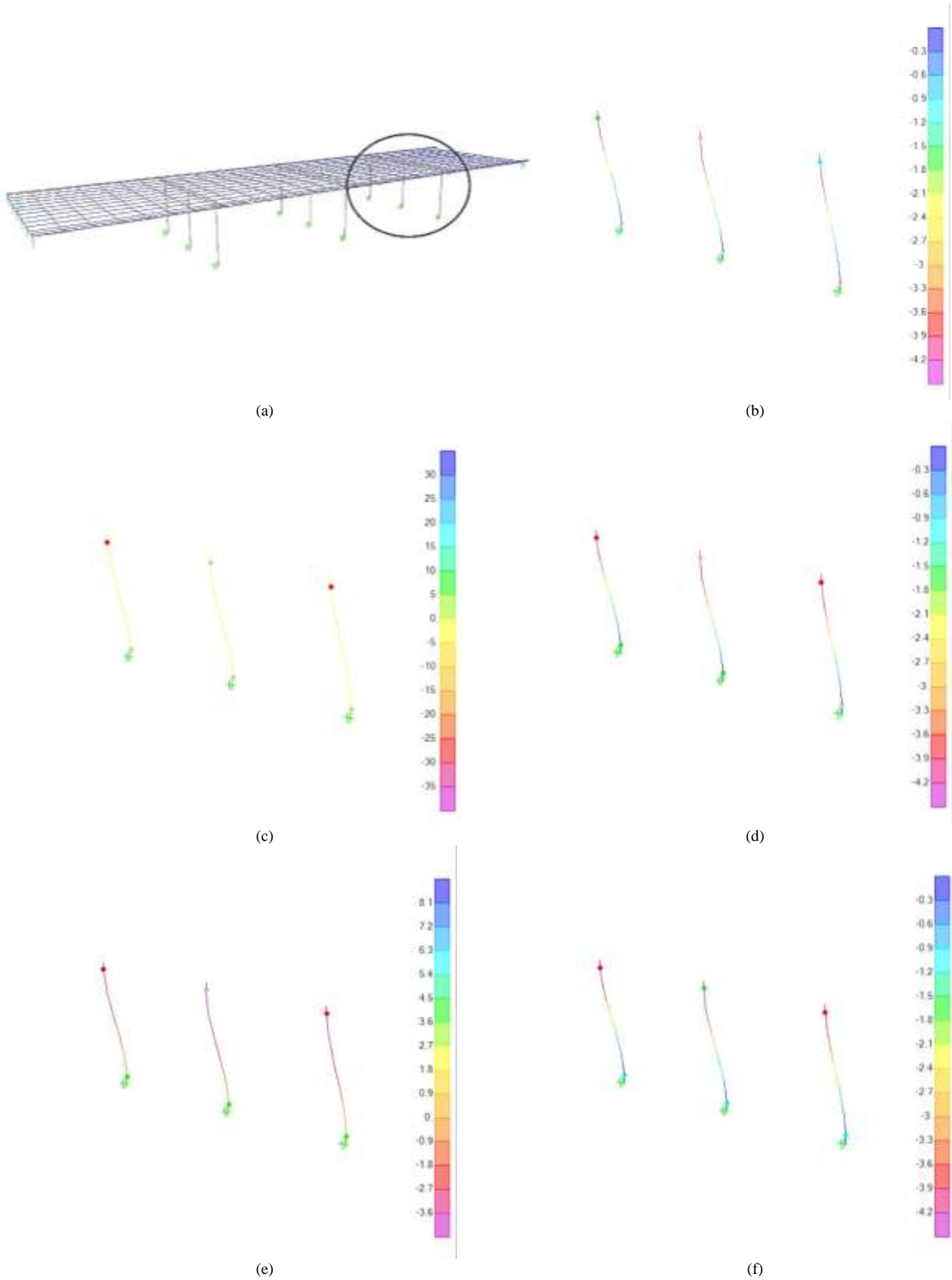
(a)

(b)

(c)

(d)

(e)

(f)

Fig 3. The plastic hinge mechanism of 8-m column bridge for nonlinear time history analysis in different steps: a) the critical pier in the bridge, b) step 0, c) step 500, d) step 1000, e) step 1500, and f) step 1800.

The inelastic performance is not frequent on bridge decks during the earthquake. In most cases, the inelastic performance occurs due to deck unseating [23]. Hence, in several past studies, the superstructure is considered to behave in elastic zoon [6, 55]. In the present study, superstructures were assumed to remain in the elastic range of behavior. This is a reasonable assumption because the seismic demands reached the plastic capacity of the deck in none of the analyses. All bridges were assumed to be located on hard soil. Therefore, soil flexibility at the bridge foundations is not considered in the analytical models. The models for confined and unconfined concrete strength parameters were considered based on Mander models [48]. On the basis of the observation of analyses obtained by the application of finite element modeling, Fig. 4 illustrates one of the selected bridge deformations by earthquake load.
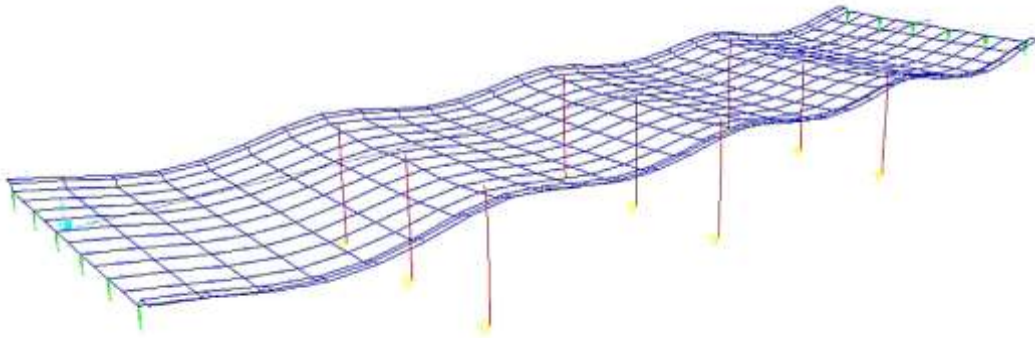

Fig 4. Deformation of one of the selected bridges

3.2. Ground Motion Selection

Selecting appropriate ground motions is one of the essential steps for the probabilistic seismic safety assessment of structures. The strong ground motion (SGM) station site condition should be compatible with the considered structures. Since all bridges are rested on hard soil, SGMs were selected within those recorded on relatively stiff soils having $V_s \geq 360$ m/s. Moreover, the attempt was made to select the ground motions of PGA>0.1g and the moment magnitude M_w>5.0. In this study, only far-field earthquakes with R< 15 Km belonging to strike-slip and reverse faults were considered. Forty SGM records, including 20 strike-slip and 20 reverse ones, were used. The acceleration time-histories are obtained from the PEER strong-motion databases (http://ngawest2.berkeley.edu).

More detail due to SGM selection is provided by Mosleh et al. in the following research studies [21]. Strong Motion Databases (Tables 3 and 4) show the significant characteristics of the selected earthquakes. Mw is moment magnitude in these tables, R is an epicentral distance, PGA is Peak Ground Motion and ASI is Acceleration Spectral Intensity. These horizontal orthogonal components are used for response history analyses. The response spectrum of each ground motion is calculated, considering the square root of the sum of the squares (SRSS) of the response spectrum of the two horizontal ground motion components. More details about the ASI calculation are provided in the following research [14]. Fig. 5 presents the response spectra of 5% damped SGMs for strike-slip and reverse records.

Table 3
Some parameters of the SGMs belonging to reverse seismic sources

Main event	Year	M_w	R (Km)	PGA (g)	ASI (g*s)
Chi-Chi	1999	7.62	101.62	0.11	0.491
Chi-Chi	1999	7.62	63.29	0.13	0.579
Chi-Chi	1999	7.62	37.83	0.17	0.815
Chi-Chi	1999	7.62	47.86	0.20	0.968
Chi-Chi	1999	7.62	39.70	0.26	0.9498
Chi-Chi	1999	7.62	86.39	0.36	1.119
Chi-Chi	1999	7.62	95.70	0.52	1.066
Chi-Chi	1999	7.62	59.80	0.08	0.394
Northridge	1994	6.69	14.92	0.21	0.760
Northridge	1994	6.69	18.62	0.39	0.647
Northridge	1994	6.69	39.39	0.47	0.568
Northridge	1994	6.69	40.68	0.49	1.693
Northridge	1994	6.69	16.27	0.51	0.890
Northridge	1994	6.69	22.45	0.59	0.976
Sanfernando	1971	6.61	25.36	0.30	0.619
Whittier Narrows	1987	5.99	21.26	0.34	0.516
Capemendocino	1992	7.01	53.34	0.17	0.568
Capemendocino	1992	7.01	22.64	0.42	1.278
Tabas	1978	7.40	20.63	0.35	0.767
Tabas	1978	7.40	55.24	0.81	2.281

Table 4
Some parameters of the SGM, strike-slip fault

| Main event	Year	M_w	R (Km)	PGA(g)	ASI (g*s)
Morgan Hill	1984	6.19	30.05	0.10	0.285
Parkfield	2004	6.00	14.50	0.47	0.447
Parkfield	2004	6.00	14.80	0.60	0.624
Manjil	1990	7.40	40.43	0.50	0.986
Morgan Hill	1984	6.19	36.34	0.28	0.790
Morgan Hill	1984	6.19	16.67	0.34	0.847
Kobe	1995	6.90	18.27	0.71	2.794
Imperial Valley	1979	6.53	24.82	0.18	0.580
Duzce	1999	7.14	27.74	0.14	0.356
Victoria	1980	6.33	33.73	0.5722	0.998
Parkfield	1966	6.19	40.26	0.2934	0.480
Landers	1992	7.28	27.33	0.1407	0.560
Landers	1992	7.28	82.12	0.3733	1.100
Kobe	1995	6.90	123.33	0.0765	0.166
Duzce	1999	7.14	29.27	0.2101	0.479
Duzce	1999	7.14	24.05	0.7367	0.806
Parkfield	2004	6.00	32.10	0.2710	1.180
Imperial Valley	1979	6.53	48.62	0.1661	0.330
Duzce	1999	7.14	31.56	0.1174	0.297
Duzce	1999	7.51	77.63	0.1387	0.682

(a)   (b)
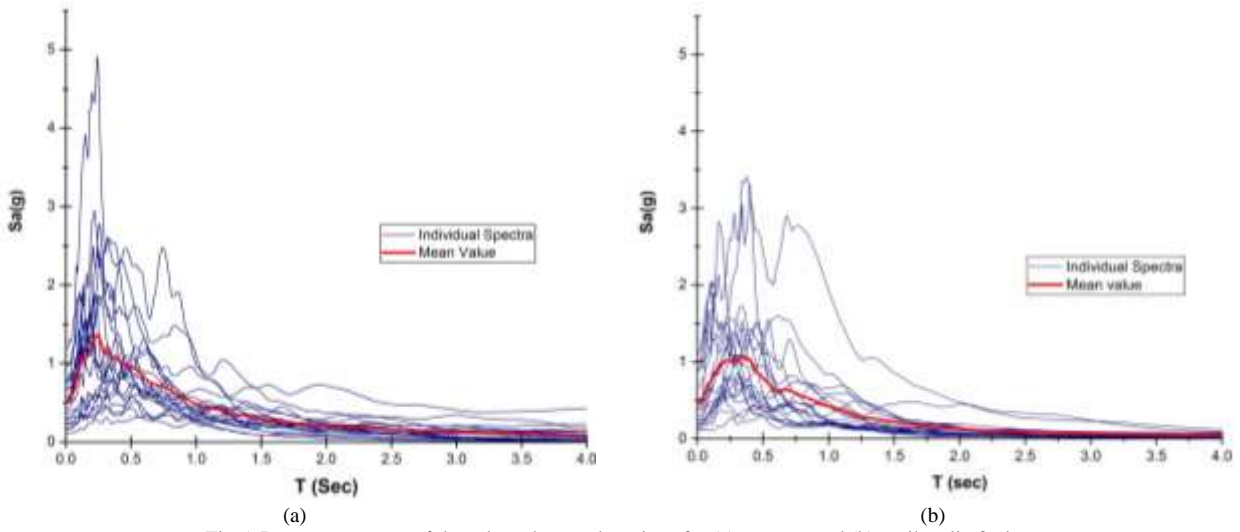
Fig 5. Response spectra of the selected ground motions for (a): reverse and (b): strike-slip faults.

4. Nonlinear Response History Analyses

The development of analytical fragility curves requires large amounts of data and nonlinear numerical analysis. Nonlinear analyses are generally time-consuming and may be impossible in particular cases because of convergence problems. However, the use of soft computing techniques, such as neural prediction algorithms, can be promising. Artificial Neural Networks (ANN) are a branch of soft computing which often employed for data prediction, filtering, and clustering. Because of their wide applications, artificial neural networks are increasingly employed in various engineering disciplines [40, 56, 57]. ANNs are powerful mathematical tools to simulate complex systems for predicting purposes [58]. During recent decades, several researchers applied ANN for simulating complex Structural Engineering problems [25, 59-63].

4.1. Theoretical Background

Various types of ANN are available, among which multilayer perceptron (MLP) networks are the most common. Every MLP neural network includes an input layer, one or more hidden layers, and an output layer (See Fig. 6). Each layer consists of artificial neurons interconnected to the neurons of the adjacent layer. The artificial neurons of the input layer get the data from the environment. Meanwhile, the neurons of other layers achieve the data from other neurons. In such neurons, the input data is the output of the connected neuron, which multiplies to a particular variable weight (so-called synaptic strength) [64]. Every neuron is associated with a function that operates on its input(s). In the present study, Feed Forward [59] MLP neural prediction approach was employed. MLP networks are the most typical types of neural networks, which are frequently applied in solving Structural and Earthquake Engineering problems. Neural network information passes from the input layer to the output one through hidden layer(s). Artificial neural networks require learning algorithms for predicting. The back-propagation technique is one of the most appropriate learning algorithms for MLP networks [41]. The connecting path of two particular neurons in neighboring layers is associated with a certain variable weight, so-called synaptic strength. The input to a neuron is calculated by multiplying the output of the connected neuron by their synaptic strength. Finally, all the weighted inputs to the neuron are summed up as follows:

$$net_j = \sum_{i=1}^{n} x_i W_{ij} \qquad (9)$$

Where n is the total number of input data to neuron j, x_i is the output variable of neuron i and W_{ij} is the synaptic strength of neurons i and j. Every neuron is associated with a threshold value and squashing function. By exceeding net_j from the threshold value,

the squashing function will be activated. Depending on the nature of the problem (e.g., the range of output values), different types of mathematical functions can be used as a squashing function. In this study, a sigmoidal function has been utilized. Therefore, the output of neuron j can be calculated as follows:

$$y_j = f(net_j) = \frac{1}{1 + exp(-net_j)} \qquad (10)$$

Every neural network is associated with a learning algorithm. In the present study, the back-propagation algorithm is employed. In such a network, the final goal of training is to calculate the synaptic strengths of links connecting the nodes utilizing the training examples set. To this end, the errors between the calculated outputs from the existing ones should be calculated and iteratively minimized. Different learning rules are available to specify how the synaptic strengths are modified in each of the iterations. The back-propagation technique is based on the modification of the synaptic strength in the output-input direction. By feeding the input-output sets to the network, the computational error can be calculated based on the difference between the calculated output and the desired one. The synaptic strengths will be corrected in a susceptive way in the backward direction. The back-propagating procedure is stopped when the computational error is less than the predefined acceptable error. In this study, the Levenberg–Marquardt method [65, 66] is employed, which is a robust form of the back-propagation algorithm.
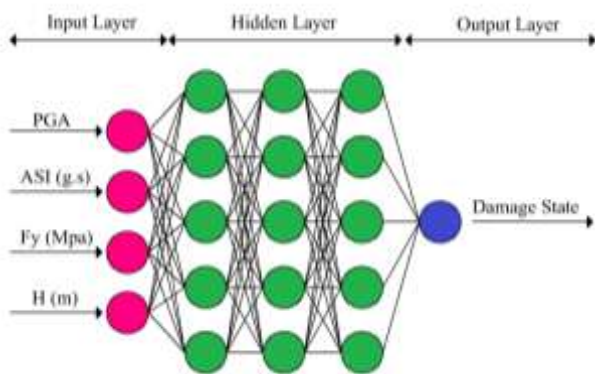

Fig 6. MLP structure

4.2. Structure of ANN

In this study, the yield strength of reinforcing bars (F_y), the bridge column height (H), PGA and acceleration spectral intensity (ASI) parameters were considered as network input and the damage state (DS) of bridges was considered as the output. The results of numerical analyses were splited into two groups. 70% of the input-output sets have been used to train the ANN, while the remained 30% have been employed to validate the neural network. The most relatively appropriate structure of the MLP network was selected based on the Least Mean Square Error (MSE) and the maximum correlation coefficient of the fitting curve (R^2). Different structures of MLP networks were designed and their associated MSE and R^2 were calculated. A structure associated with the least MSE and the highest R^2 was selected as the most relatively appropriate network. It should be noted that MSE and R^2 can be calculated using Eqs. 11 and 12 respectively:

$$MSE = \frac{1}{m} \sum_{i=1}^{m} e_i^2 \qquad (11)$$

$$R^2 = 1 - \frac{\sum_{i=1}^{m}(t_i - o_i)^2}{\sum_{i=1}^{m}(o_i)^2} \qquad (12)$$

where m is the number of tries, t is the target value, o is the output value, t_i is the target of prediction as o_i is its corresponding neural prediction.

After determining the proper structure for the neural network and network training, it is necessary to verify the network results. For this purpose, the neural network predictions were compared to the test samples, which were the results of numerical analyses. Some of the comparisons of numerical results and neural predictions are presented in Figure 7, considering different column heights, yield strength of reinforcing bars and seismic source. It should be noted that for the selected structure, R^2 and MSE are calculated as 0.82 and 0.187, respectively. As shown in Fig. 7, neural predictions are consistent with the results of numerical analyses. Hence, the designed structure of the MLP neural network is capable of predicting new bridge-earthquake cases. Ensuring the appropriate performance of the neural network, the network was

used to simulate new earthquake-bridge samples. Accordingly, the neural network generated 400 new bridge performance data.
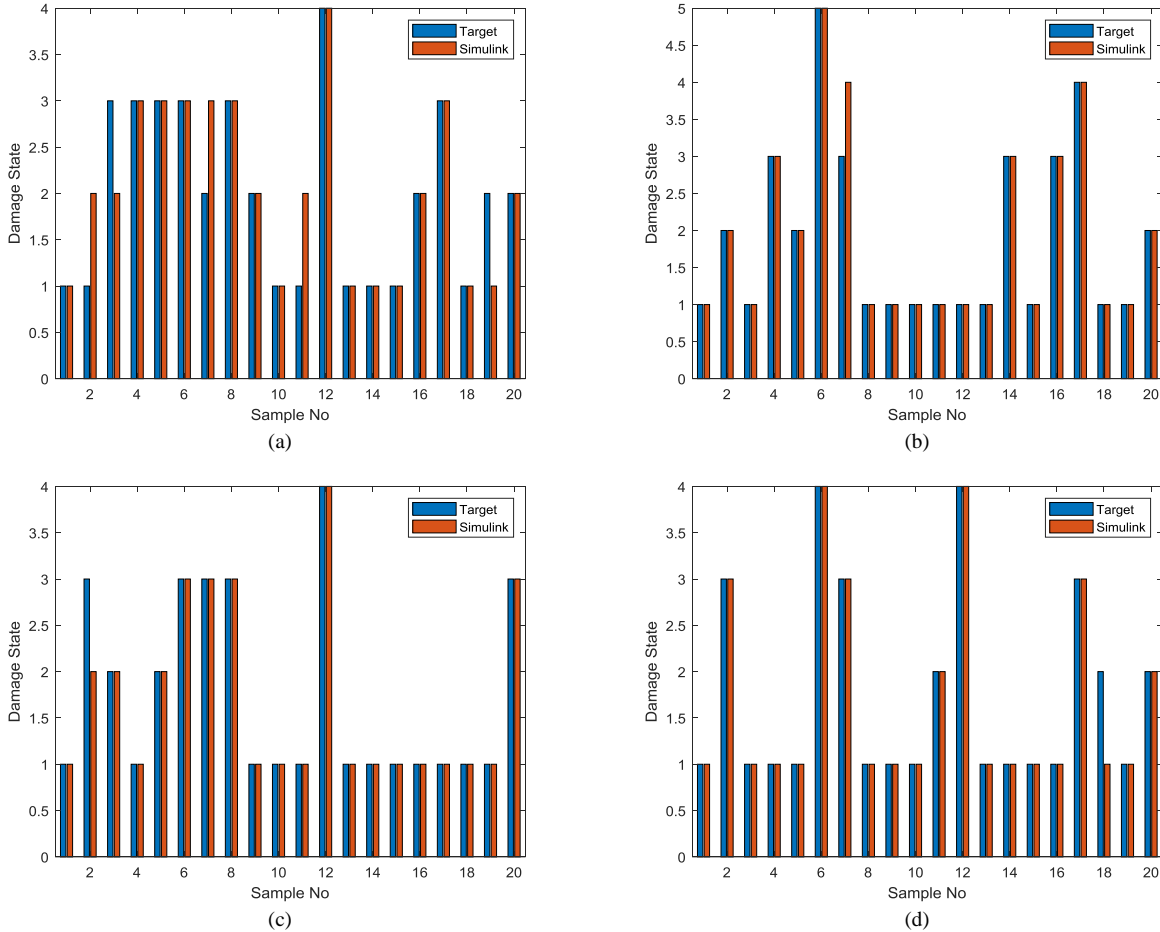

(a)

(b)

(c)

(d)

Fig 7. Comparison of network prediction to the results of response history analyses (a): 8-meter bridge with $F_y = 300$Mpa for reverse fault for transverse direction, (b): 8-meter bridge with $F_y = 300$ Mpa for strike-slip fault for transverse direction, (c): 4-meter bridge with $F_y = 392$Mpa for reverse fault for transverse direction, (d): 6-meter bridge with $F_y = 392$Mpa for a reverse fault along the longitudinal direction

5. Fragility Analysis

Fragility curves are functions, which quantify the seismic performance of a particular structure in a probabilistic platform. In other words, fragility curves illustrate the probability of reaching or exceeding a particular damage state in terms of an intensity measure (IM) of the ground motion (e.g., PGA) [24]. Hence, seismic fragility curves can be formulized as follows:

$$Fragility = P\left[\frac{D}{C} \geq 1 \mid IM\right]$$

13

in which P is a probabilistic function, D is seismic demand and C is the capacity of the structure.

5.1. Definition of Damage States

Defining the proper damage states is an essential step to perform the fragility curves of structures. The seismic performance of bridges during the recent

earthquakes has shown that the main failure mode of bridges is mostly related to damage to of the piers. Many bridge failure modes are directly or indirectly dependent on column failure. Therefore, many researchers employ the performance characteristics of the columns to calculate the damage states of the bridge [13, 25, 67, 68].

The columns of the bridge are one of the most vulnerable parts of the bridge that can be damaged during an earthquake. Although failure may occur elsewhere in bridges, this study aims to reduce the column bridge damage. There are different methods to classify bridge vulnerabilities ATC13 [11].

In the basis of HAZUS [69], five levels of damage states are used for bridges, ranging from no damage to a bridge collapse. In the present study, according to the Hwang method [67] four limit states have been defined for bridges, from slight to collapse. In order to quantify the defined damage states, displacement ductility was employed considering Hwang methodology [68]. The displacement ductility ratio is defined as:

$$\mu_{di} = \frac{\delta_i}{\delta_1} \tag{14}$$

in which μ_{di} is the displacement ductility ratio for the damage state i, δ_i is the relative displacement at the top of a column at the corresponding damage state i and δ_1 is the relative displacement of a column corresponding to the first yield of reinforcing bars:

$$\delta_1 = \frac{q}{3} \varphi_1 L^2 \tag{15}$$

where L is considered as the distance between the location of the plastic hinge to contra-flexure point of column and φ_1 is defined as the curvature of the first yield of longitudinal bars in the column as depicted in Fig. 8. It should be noted that for the transversal motion of the bridge $q=1$ and for in longitudinal response $q=2$.

According to Eq.14, the displacement ductility ratio for the first yield of the column is $\mu_{d1} = 1$. μ_{d1} is the first damage state of bridge piers. The second

limit state (μ_{d2}) is corresponding to the plastic hinge formation in columns and can be calculated as follows:

$$\mu_{d2} = \frac{q}{3} \frac{\varphi_2 L^2}{\delta_1} \tag{16}$$

where φ_2 is the defined as a curvature corresponding to the yield point of a column (See Fig. 8). Moreover, the displacement ductility for the third damage state (μ_{d3}) can be achieved by the following equation [68]:

$$\mu_{d3} = \frac{q/3(\varphi_2 L^2) + \theta_p(L + 0.5L_p)}{\delta_1} \tag{17}$$

where L_p and , θ_p denote the length and the rotation of the plastic hinge respectively, and can be estimated as follows [51] :

$$L_p = 0.08L + 0.022f_{ye}d \geq 0.044f_{ye}d \tag{18}$$

$$\theta_P = (\varphi_{3-} \varphi_2)L_p \tag{19}$$

in which d is the diameter of the longitudinal reinforcing bars, L is the distance from the plastic hinge to the inflection point and f_{ye} is the effective yield strength of the reinforcing bars. φ_3 is the curvature of a column when $\varepsilon_c=0.002$ or $\varepsilon_c=0.004$ for the columns with or without lap splices. In this study both of these values were considered. Moreover, ε_c is the maximum compressive strain in the column cross-section. Finally, according to [68], the last limit state, corresponded to the bridge collapse, is $\mu_{d4} = \mu_{d3} + 3$ [70].
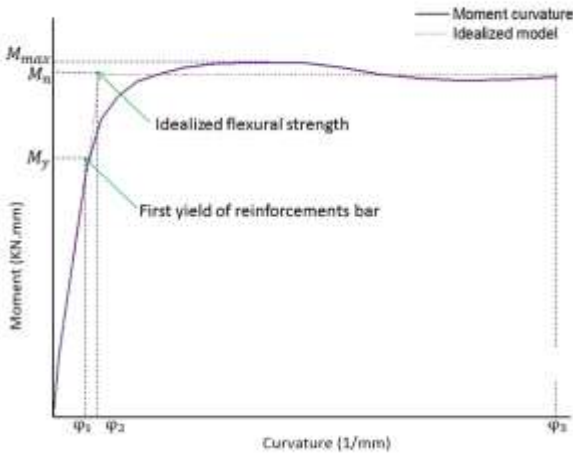
Fig 8. Moment-curvature diagram of columns

5.2. Selecting an Intensity Measure

Selecting an appropriate intensity measure (IM) is an essential step to develop reliable seismic fragility curves. There is a considerable lack of studies in the literature regarding the selection of appropriate IM to perform the fragility curves of bridges. A proper IM for fragility analysis should be sufficient so that its adoption results in relatively small variations in the seismic response of a structure for a certain IM level [71]. Moreover, the distribution of structural response for the selected IM should be independent of other parameters involved to calculate seismic hazard [72]. Most of the previous researchers utilized a single intensity measurement (IM) to develop fragility functions. Peak Ground Motion (PGA) and Spectral acceleration (Sa) are two of the most frequently used IMs for fragility analysis of bridges as they are easier to understand and more comparable [25, 33, 73]

In this study, PGA and acceleration spectral intensity (ASI) were used as IM for fragility analysis. It should be noted that for a category of structures where their periods ranging between T_i and T_f, ASI is defined as:

$$ASI = \int_{T_1}^{T_2} Sa(T,\xi)dT \tag{20}$$

In order to calculate the *ASI* of each SGM, the SRSS of the *Sa* of both horizontal components of the selected record was utilized. Furthermore, for the selected category of bridges, T_1 and T_2 are 0.28 Sec and 0.58 Sec respectively.

5.3. Development of Analytical Fragility Curves

Each bridge was subjected to two orthogonal horizontal components of the ground motions. The maximum absolute ductility demand determines the damage limit state of the bridge column for each seismic record. The number of bridges that reach or exceed a specified damage limit state is obtained by subjecting the models under the seismic records with a certain intensity measure (PGA and ASI). The intensity measures consider the SRSS of the two horizontal components of the ground motions. Several researches, as well as this study, adopt the lognormal distribution to obtain fragility curves [2, 74-77]. Each fragility function depends on a median value and an associated dispersion factor (lognormal standard deviation) of ground motion, which is represented by seismic intensity measures. To select the parameters of the lognormal probability density function, the least-squares method is applied. The coefficient of determination (R^2) determines how well the fitted curve relates to the data of the fragility functions. This indicator, which varies between 0 and 1, shows how closely the lognormal distribution obtains the estimated points and the smooth curve. The closer the R^2 value is to 1, the more reliable are the estimated fragility curves. Finally, fragility functions of each bridge class are developed for the intensity measures of PGA employing the procedure described before. Table 5 indicates the typical relationship between displacement ductility capacity and column height. It shows that by increasing the column height, the plastic hinge enhances. However, since the rotation of the column end decreases, the displacement ductility diminishes as well, as explained by Priestley et al. [51]. Fig. 9 depicts the fragility curve for data from time histories analysis for ASI and PGA respectively, considering 40 selected ground motions due to reverse and strike-slip faults.

Table 5
Limit states for integral bridges

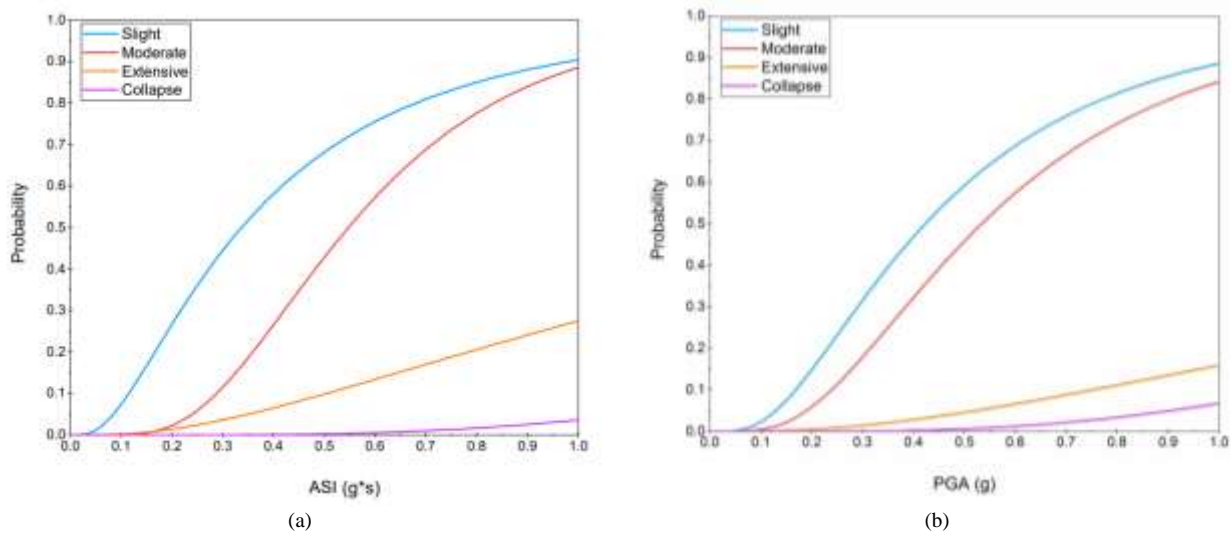| Column height (m)	4		6		8	
Fy (Mpa)	300	392	300	392	300	392
L_p (cm)	325	375	404	455	484	534
φ_1	0.0029	0.0037	0.003	0.0037	0.003	0.0041
φ_2	0.0035	0.0044	0.0035	0.0044	0.0035	0.0045
φ_3	0.0145	0.0141	0.0143	0.014	0.0142	0.0121
μ_{d2}	1.21	1.19	1.17	1.19	1.17	1.10
μ_{d3}	2.91	2.53	2.52	2.28	2.38	1.79
μ_{d4}	5.91	5.53	5.52	5.28	5.38	4.79

(a)   (b)

Fig 9. The comparison of fragility curves for different damage limit states, (a): ASI, (b): PGA

5.4. Development of Hybrid Fragility Curves

The accuracy and efficiency of seismic fragility functions are remarkably dependent on the accuracy and sufficiency of the available data in datasets. In other words, larger datasets are required to derive more effective fragility functions. Inadequate information in databases may lead to unreasonable scatter in the results of fragility analyses [24, 78]. Hence, the development of an accurate analytical fragility curve requires a noticeable number of nonlinear analyses. As an enormous number of nonlinear analyses is costly and sometimes impossible (due to convergence problems), ANN-based simulations can be used to increase the number of available data. Accordingly, the neural predictions of the selected ANN of section 4.2 were added to the available database to prepare a hybrid dataset from neural predictions and results of numerical analyses. The hybrid fragility curves are illustrated in Fig. 10. Four limit states are identified in Fig. 10, including slight, moderate, extensive, and collapse.
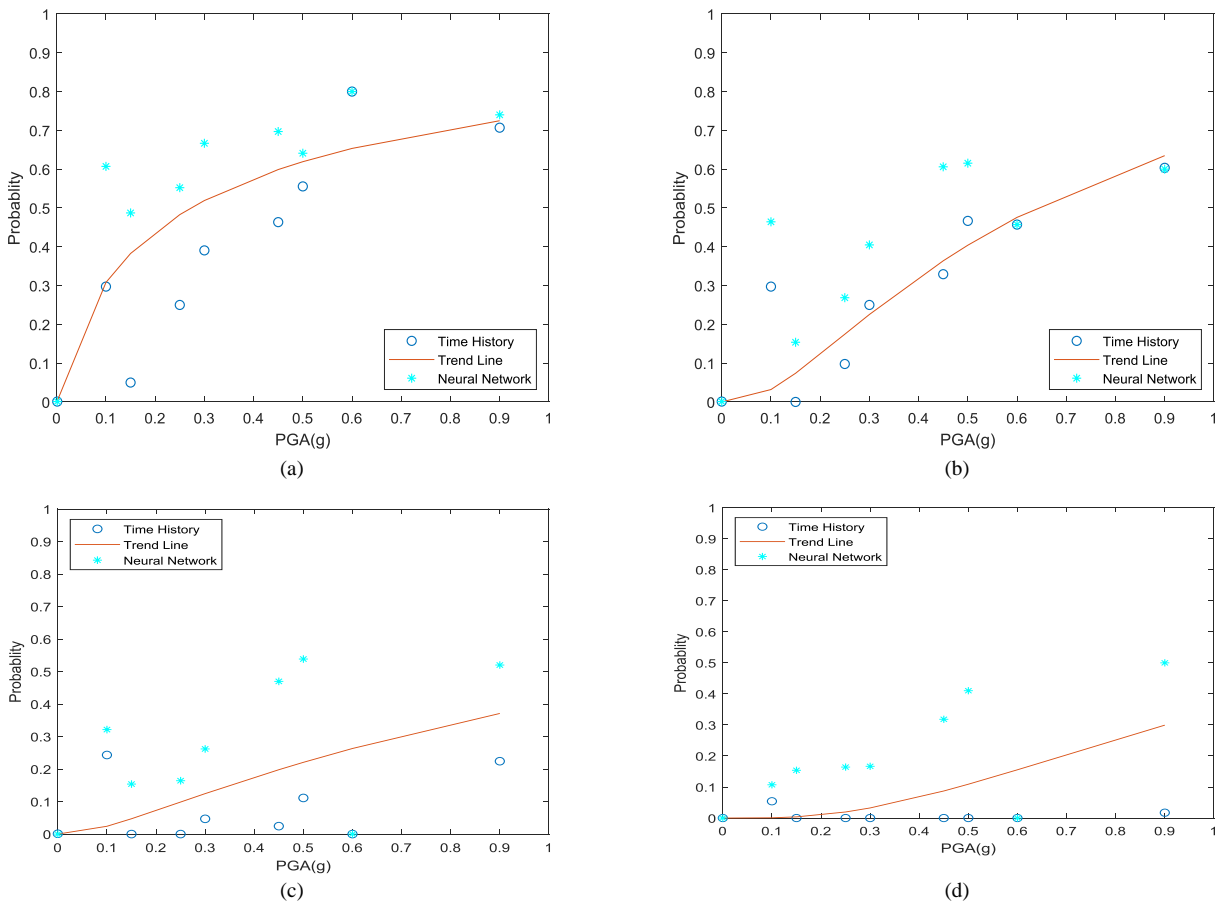
Fig 10. Hybrid fragility curves, a) Slight, b) Moderate, c) Extensive, d) Collapse

5.5. Comparison of Analytical and Hybrid Fragility Curves

In Tables 6 and 7, the correlation coefficient of the PGA-based and ASI-based fragility curves are tabulated for analytical and hybrid curves. As indicated in Tables 6 and 7, the correlation coefficients of damage states 1 and 2 were not improved in hybrid fragility curves. On the other hand, for damage states 3 and 4, in which analytical fragility curves were associated with relatively unreasonable correlation coefficients, hybrid curves

had considerably more reasonable correlation coefficients. The tables also show that PGA-based fragility curves are associated with relatively greater correlation coefficients than ASI-based ones. Fig. 11 illustrates the comparison of analytical and hybrid fragility curves constructed in terms of PGA and ASI. From the results presented in Tables 6 and 7, it is possible to infer that neural network data significantly improve the fragility curves for damage states 3 and 4.

Table 6
The correlation coefficient of fragility curve in PGA

Earthquake parameter	state	Damage state	correlation coefficient
PGA	Without the use of neural network production data	DS1	0.93
		DS2	0.89
		DS3	0.43
		DS4	0.13
	Using Neural Network Manufacturing Data	DS1	0.93
		DS2	0.83
		DS3	0.48
		DS4	0.63

Table 7
The correlation Coefficient of fragility Curve Based on Seismic Spectrum

Earthquake parameter	state	Damage state	correlation coefficient
ASI	Without the use of neural network production data	DS1	0.85
		DS2	0.8
		DS3	0.33
		DS4	0.15
	Using Neural Network Manufacturing Data	DS1	0.87
		DS2	0.85
		DS3	0.46
		DS4	0.61

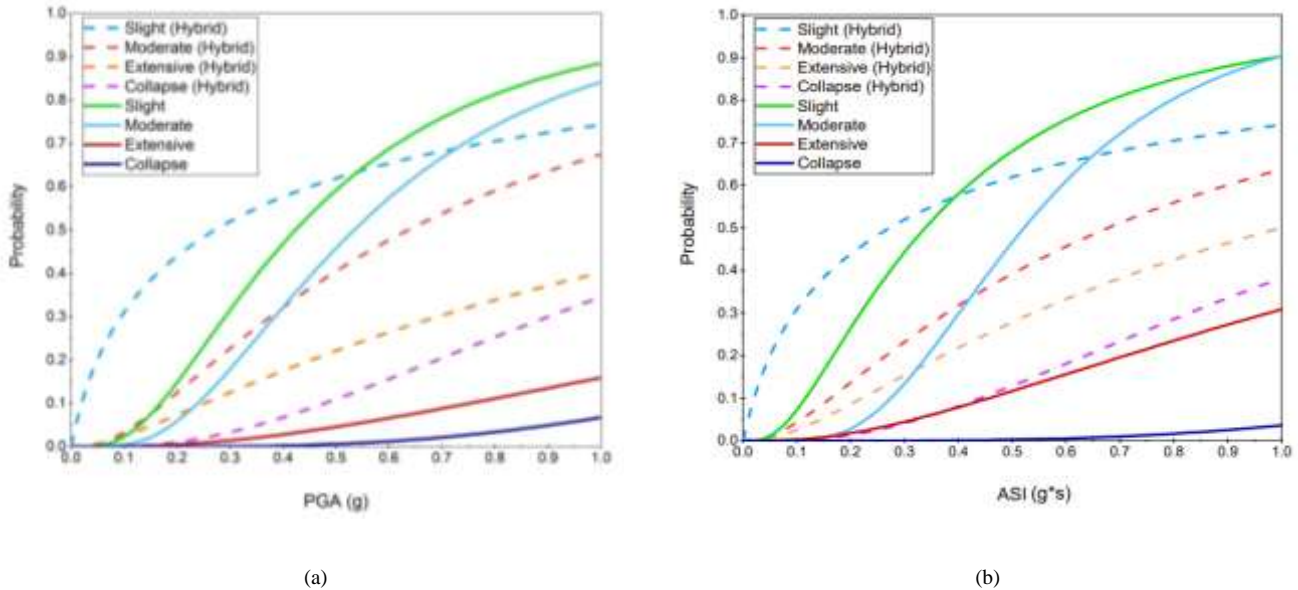(a)   (b)

Fig 11. The comparison of analytical and hybrid fragility curves developed in terms of (a) PGA and (b) ASI.

6. Conclusions

Nonlinear analyses are time-consuming and require a considerable amount of computer memory. They may also encounter convergence problems. Meanwhile, to achieve a reliable fragility curve, remarkable numbers of nonlinear analyses are required. Therefore, the development of fragility curves using nonlinear analysis is expensive, computationally time-consuming and sometimes impractical, mainly when complex structures such as bridges are analyzed. Therefore, soft computing techniques such as artificial neural networks seem to be proper alternatives due to their ability to reduce the number of analyzes in parametric studies

In this research, the development of fragility curves for a series of RC bridges was investigated. Fragility curves are obtained based on three-dimensional analytical bridge models, a set of ground motion records from reverse and strike faults, and a complete analysis of the nonlinear response history. For this purpose, two kinds of analytical and hybrid curves were developed. In order to derive analytical fragility curves, response history analyzes were employed. In addition, using a trained artificial neural network with analytical data, the seismic performance of the bridges is predicted. The yield stress of reinforcing bars (Fy), the bridge height (H) as well as PGA and ASI, were considered as the input vectors of the artificial neural networks (ANN). To this end, 1032 data were obtained.

From history analysis outputs, 70% of data were used for network training and the remained (30%) were employed for network testing. Finally, using 400 artificial neural network data in a wide variety of bridges of this study, network performance and results from data in the development fragility curve were investigated. The results revealed that neural prediction is an appropriate procedure for predicting the bridges studied in this study. Furthermore,

reducing the number of required response history analyses is proper to come by a precise fragility function.

Furthermore, the efficiency of the neural prediction in the development of fragility curves for damage stats 3 and 4 (extensive and collapse) was considerably better than that for damage stats 1 and 2 (slight and moderate). In other words, neural network simulation can efficiently improve fragility curves with notable scattered data. This study also showed that the PGA-based fragility curves were associated with higher correlation coefficients compared to ASI-based ones.

7.Acknowledgments

References

[1] Avsar, O., Yakut, A., Caner, A., Analytical Fragility Curves for Ordinary Highway Bridges in Turkey. Earthquake Spectra, 2011. **27**(4): p. 971-996. doi: 10.1193/1.3651349.

[2] Banerjee, S., Shinozuka, M., Nonlinear static procedure for seismic vulnerability assessment of bridges. Computer-Aided Civil and Infrastructure, 2007. **22**(4): p. 293-305. doi: 10.1111/j.1467-8667.2007.00486.x.

[3] Choine, M., Connor, A., Padgett, J., Comparison between the Seismic Performance of Integral and Jointed Concrete Bridges. Journal of Earthquake Engineering, 2015. **19**(1): p. 172-191. doi: 10.1080/13632469.2014.946163.

[4] Eshghi, S. and M. Razzaghi, Performance of industrial facilities in the 2003 Bam, Iran, earthquake. Earthquake Spectra, 2005. **21**(1): p. 395-410. doi: 10.1193/1.2098810.

[5] Billah, A.H.M.M., Alam, M.S., Bhuiyan, A.R., Fragility analysis of retrofitted multi-column bridge bent subjected to near fault and far field ground motion. ASCE Journal of Bridge Engineering, 2013. **18**(10): p. 992–1004. doi: 10.1061/(ASCE)BE.1943-5592.0000452.

[6] Mander, J., Dhakal, R., Mashiko, N., Solberg, K., Incremental dynamic analysis applied to seismic financial risk assessment of bridges. Engineering Structures, 2007. **29**(10): p. 2662–2672. doi: 10.1016/j.engstruct.2006.12.015.

[7] Pan, H., et al., Time-frequency-based data-driven structural diagnosis and damage detection for cable-stayed bridges. Journal of Bridge Engineering, 2018. **23**(6): p. 04018033. doi: 10.1061/(ASCE)BE.1943-5592.0001199.

[8] Tavares, D.H., Padgett, J.E., Paultre, P., Fragility curves of typical as-built highway bridges in eastern Canada. Engineering Structures, 2012. **40**: p. 107–118. doi: 10.1016/j.engstruct.2012.02.019.

[9] Yazdani, M., V. Jahangiri, and M.S. Marefat, Seismic performance assessment of plain concrete arch bridges under near-field earthquakes using incremental dynamic analysis. Engineering Failure Analysis, 2019. **106**: p. 104170. doi: 10.1016/j.engfailanal.2019.104170.

[10] Yazgan, U., Empirical seismic fragility assessment with explicit modeling of spatial ground motion variability. Engineering Structures, 2015. **100**(1): p. 479–489. doi: 10.1016/j.engstruct.2015.06.027.

[11] ATC, Seismic vulnerability and impact of disruption of life lines in the Coterminous United States. (Report No. ATC-25). 1991: Redwood City, CA: Applied Technology Council.

[12] Avsar, O., FRAGILITY BASED SEISMIC VULNERABILITY ASSESSMENT OF ORDINARY HIGHWAY BRIDGES IN TURKEY, in Civil Engineering Department. 2009, MIDDLE EAST TECHNICAL UNIVERSITY.

[13] Manjily, F., A. Mosleh, and M. Razzaghi, Seismic fragility of concrete bridges designed to current and older AASHTO specifications. Proceedings of the Institution of Civil Engineers-Structures and Buildings, 2021: p. 1-30. doi: 10.1680/jstbu.19.00237.

[14] Mosleh, A., J. Jara, M. Razzaghi, H. Varum., Probabilistic Seismic Performance Analysis of RC Bridges. Journal of Earthquake Engineering, 2020. **24**(11): p. 1704–1728. doi: 10.1080/13632469.2018.1477637.

[15] Whitman, R.V., Biggs, J.M., Brennan, J.E., Cornell, A.C., Neufville, R.L., Vanmarcke, E.H., Seismic design decision analysis. ASCE Journal of Structural Division, 1975. **101**(5): p. 1067–1084. doi: 10.1061/JSDEAG.0004049.

[16] Veneziano, D., F. Casciati, and L. Faravelli, Method of seismic fragility for complicated systems, P.m.i.s.r.a.f.n.p.p. proceedings, Editor. 1983: MIT, Cambridge, MA.

[17] Del Gaudio, C., et al., Seismic fragility for Italian RC buildings based on damage data of the last 50 years. Bulletin of earthquake engineering, 2020. **18**(5): p. 2023-2059. doi: 10.1007/s10518-019-00762-6.

[18] Rossetto, T. and A. Elnashai, Derivation of vulnerability functions for European-type RC structures based on observational data. Engineering structures, 2003. **25**(10): p. 1241-1263. doi: 10.1016/S0141-0296(03)00060-9.

[19] Miano, A., et al., Empirical fragility assessment using conditional GMPE-based ground shaking fields: Application to damage data for 2016 Amatrice

Earthquake. Bulletin of Earthquake Engineering, 2020. **18**(15): p. 6629-6659. doi: 10.1007/s10518-020-00945-6.

[20] Shinozuka, M., et al., Nonlinear static procedure for fragility curve development. Journal of engineering mechanics, 2000b. **126**(12): p. 1287-1295. doi: 10.1061/(ASCE)0733-9399(2000)126:12(1287).

[21] Mosleh, A., Seismic vulnerability assessment of existing concrete highway Iranian bridges, in Civil Engineering Department. 2016, Aveiro University, Aveiro, Portugal.

[22] Nielson, B.G., DesRoches, R., Analytical seismic fragility curves for typical bridges in the Central and Southeastern United States. Earthquake Spectra, 2007a. **23**(3): p. 615–633. doi: 10.1193/1.2756815.

[23] Ramanathan, K., DesRoches, R., Padgett, J.E. , Analytical fragility curves for multispan continuous steel girder bridges in moderate seismic zones. Transportation Research Record, 2010. **2202**(1): p. 173-182. doi: 10.3141/2202-21.

[24] Razzaghi, M.S., Eshghi, S., Probabilistic seismic safety assessment of precode cylindrical oil tanks. J Performance of Constructed Facilities. Journal of Performance of Constructed Facilities, 2014. **29**(6). doi: 10.1061/(ASCE)CF.1943-5509.0000669.

[25] Razzaghi, M., M. Safarkhanlou, A. Mosleh, P. Hosseini., Fragility assessment of RC bridges using numerical analysis and artificial neural networks. Earthquakes and Structures, 2018. **15**(4): p. 431-441. doi: 10.12989/eas.2018.15.4.431.

[26] Choi, E., DesRoches, R., Nielson, B., Seismic fragility of typical bridges in moderate seismic zones. Engineering Structures, 2004. **26**(2): p. 187-199. doi: 10.1016/j.engstruct.2003.09.006.

[27] Loh, C.H., Liao, W. I., Chai, J. F., Effect of near-fault earthquake on bridges: lessons learned from Chi-Chi earthquake. Earthquake Engineering and Engineering Vibration, 2002. **1**(1): p. 86-93. doi: 10.1007/s11803-002-0011-3.

[28] Mitropoulou, C.C. and M. Papadrakakis, Developing fragility curves based on neural network IDA predictions. Engineering Structures, 2011. **33**(12): p. 3409-3421. doi: 10.1016/j.engstruct.2011.07.005.

[29] Monti, G., Nistico, N., Simple probability-based assessment of bridges under scenario earthquakes. Journal of Bridge Engineering, 2002. **7**(2): p. 104-114. doi: 10.1061/(ASCE)1084-0702(2002)7:2(104).

[30] Mosleh, A., Razzaghi, M., Jara, j., Varum, H., Seismic Fragility Analysis of Typical Pre-1990 Bridges due to Near and Far-Field Ground Motions. International Journal of Advanced Structural Engineering and Mechanics, 2016. **8**(1): p. 1-9. doi: 10.1007/s40091-016-0108-y.

[31] Nateghi, F., Shahsavar, V.L., Development of Fragility and Reliability Curves for Seismic Evaluation of a Major Prestressed Concrete Bridge, in 13th World Conference on Earthquake Engineering. 2004: Vancouver, B.C. Canada.

[32] Ramanathana, K., Padgettb, J., DesRoches, R., Temporal evolution of seismic fragility curves for concrete box-girder bridges in California. Engineering Structures, 2015. **97**(15): p. 29-46. doi: 10.1016/j.engstruct.2015.03.069.

[33] Shinozuka, M., Feng, M.Q., Lee, J., Naganuma, T., Statistical analysis of fragility curves. Journal of Engineering Mechanics, 2000a. **126**(12): p. 1224-1231. doi: 10.1061/(ASCE)0733-9399(2000)126:12(1224).

[34] Siqueiraa, G., Sandab, A., Paultreb, P., Padgettc, J., Fragility curves for isolated bridges in eastern Canada using experimental results. Engineering Structures, 2014. **74**(1): p. 311-324. doi: 10.1016/j.engstruct.2014.04.053.

[35] Hasanzadehshooiili, H., A. Lakirouhani, and A. Šapalas, Neural network prediction of buckling load of steel arch-shells. Archives of Civil and Mechanical Engineering, 2012. **12**(4): p. 477-484. doi: 10.1016/j.acme.2012.07.005.

[36] Han, H.-G., Q.-l. Chen, and J.-F. Qiao, An efficient self-organizing RBF neural network for water quality prediction. Neural networks, 2011. **24**(7): p. 717-725. doi: 10.1016/j.neunet.2011.04.006.

[37] Feng, N., et al., A probabilistic process neural network and its application in ECG classification. IEEE Access, 2019. **7**: p. 50431-50439.

[38] Melin, P., et al., A new neural network model based on the LVQ algorithm for multi-class classification of arrhythmias. Information sciences, 2014. **279**: p. 483-497. doi: 10.1016/j.ins.2014.04.003.

[39] Rafiq, M.Y., G. Bugmann, and D.J. Easterbrook, Neural network design for engineering applications. Computers & Structures, 2001. **79**(17): p. 1541-1552. doi: 10.1016/S0045-7949(01)00039-6.

[40] Razzaghi, M. and A. Mohebbi, Predicting the seismic performance of cylindrical steel tanks using artificial neural networks (ann). Acta Polytechnica Hungarica, 2011. **8**(2): p. 129-140.

[41] Adeli, H., Neural Networks in Civil Engineering: 1989–2000. Computer-Aided Civil and Infrastructure Engineering, 2001. **16**(2): p. 126-142.

[42] Bodri, B., A neural-network model for earthquake occurrence. Journal of Geodynamics, 2001. **32**(3): p. 289-310. doi: 10.1016/S0264-3707(01)00039-4.

[43] Huang, C. and S. Huang, Predicting capacity model and seismic fragility estimation for RC bridge based on artificial neural network. Structures, 2020. **27**: p. 1930-1939. doi: 10.1016/j.istruc.2020.07.063.

[44] Reyes, J., A. Morales-Esteban, and F. Martínez-Álvarez, Neural networks to predict earthquakes in Chile. Applied Soft Computing, 2013. **13**(2): p. 1314-1328. doi: 10.1016/j.asoc.2012.10.014.

[45] Bao, Z., et al., A deep learning-based electromagnetic signal for earthquake magnitude prediction. Sensors, 2021. **21**(13): p. 4434.

[46] Mohammadi, M., A. Mosleh, M. Razzaghi, AC. Pedro, C. Rui., Stochastic analysis of railway

embankment with uncertain soil parameters using polynomial chaos expansion. Structure and Infrastructure Engineering, 2022: p. 1-20. doi: 10.1080/15732479.2022.2033277.

[47] CSI. SAP2000 V-14, Integrated finite element analysis and design of structures basic analysis reference manual. 2009, Berkeley (CA, USA), Computer and structure Inc.

[48] Mander, J., M. Priestley, and R. Park, Observed stress-strain behavior of confined concrete. Journal of structural engineering, 1988. **114**(8): p. 1827-1849. doi: 10.1061/(ASCE)0733-9445(1988)114:8(1827).

[49] Caltrans, Seismic Design Criteria Version 1.7. 2013, California Department of Transportation, Sacramento, CA.

[50] Shamsabadi, A., Rollins, K.M., and Kapuskar, M., Nonlinear Soil-Abutment-Bridge Structure Interaction for Seismic Performance-based Design. J. Geotech. & Geoenviron. Eng., ASCE, 2007. **133**(6): p. 707-720. doi: 10.1061/(ASCE)1090-0241(2007)133:6(707).

[51] Priestley, M.J.N., Seible, F.,Calvi, G. M., Seismic design and retrofitting of bridges. 1996, New York: John Wiley & Sons.

[52] Shamsabadi, A., Three-Dimensional Nonlinear Seismic Soil-Abutment-Foundation Structure Interaction Analysis of Skewed Bridges, in Department of Civil and Environmental Engineering. 2007, University of Southern California: Los Angeles, CA.

[53] Stewart, P.S., Taciroglu, E., Wallace, J.W., Ahlberg, E.R., Lemnitzer, A., Rha, C., and Tehrani, P.K. , Full Scale Cyclic Testing of Foundation Support Systems for Highway Bridges, Part II: Abutment Backwalls. 2007, Department of Civil and Environmental Engineering, University of California: Los Angeles, CA.

[54] Ramalakshmi, M., Force-displacement response of bridge abutments under passive push. Materials Today: Proceedings, 2021. **43**: p. 883-887.

[55] Mangalathu, S., et al., ANCOVA-based grouping of bridge classes for seismic fragility assessment. Engineering Structures, 2016. **123**: p. 379-394. doi: 10.1016/j.engstruct.2016.05.054.

[56] Arunthavanathan, R., et al., An analysis of process fault diagnosis methods from safety perspectives. Computers & Chemical Engineering, 2021. **145**: p. 107197.

[57] Saxena, A. and A. Saad, Evolving an artificial neural network classifier for condition monitoring of rotating mechanical systems. Applied Soft Computing, 2007. **7**(1): p. 441-454. doi: 10.1016/j.asoc.2005.10.001.

[58] Hertz, J., A. Krogh, and R.G. Palmer, Introduction to the theory of neural computation. 2018: CRC Press.

[59] Caglar, N., et al., Neural networks in 3-dimensional dynamic analysis of reinforced concrete buildings.

Construction and Building Materials, 2008. **22**(5): p. 788-800. doi: 10.1016/j.conbuildmat.2007.01.029.

[60] Kameli, I., M. Miri, and A. Raji, Prediction of Target Displacement of Reinforced Concrete Frames Using Artificial Neural Networks. Advanced Materials Research, 2011. **255**: p. 255-260. doi: 10.4028/www.scientific.net/amr.255-260.2345.

[61] Lagaros, N.D. and M. Papadrakakis, Neural network based prediction schemes of the non-linear seismic response of 3D buildings. Advances in Engineering Software, 2012. **44**(1): p. 92-115. doi: 10.1016/j.advengsoft.2011.05.033.

[62] Sofi, F.A. and J.S. Steelman. Using committees of artificial neural networks with finite element modeling for steel girder bridge load rating estimation. in Structures. 2021. Elsevier.

[63] Sun, H., H.V. Burton, and H. Huang, Machine learning applications for building structural design and performance assessment: state-of-the-art review. Journal of Building Engineering, 2021. **33**: p. 101816.

[64] Mukherjee, A. and S.N. Biswas, Artificial neural networks in prediction of mechanical behavior of concrete at high temperature. Nuclear engineering and design, 1997. **178**(1): p. 1-11. doi: 10.1016/S0029-5493(97)00152-0.

[65] Levenberg, K., A method for the solution of certain nonlinear problems. Q. Appl. Math., 1944. **2**: p. 164-168. doi:10.1090/qam/10666.

[66] Mardquardt, D., An algorithm for least square estimation of parameters. J. Soc. Ind. Appl. Math, 1963. **11**: p. 431-441. doi: doi:10.1137/0111030.

[67] Hwang, H., Jernigan, J.B., Lin, Y.W., Evaluation of seismic damage to Memphis bridges and highway systems. ASCE Journal of Bridge Engineering, 2000. **5**(4): p. 322–330. doi: 10.1061/(ASCE)1084-0702(2000)5:4(322).

[68] Hwang, H., Liu, J., Chiu, Y., Seismic fragility analysis of highway bridges. 2001, Center for Earthquake Research and Information The Universityof Memphis, MAEC RR-4 Project.

[69] HAZUS, MH 2.0, Technical Manual. 1997, Washington, DC: Federal Emergency Management Agency.

[70] FHWA, Seismic Retrofitting Manual for Highway Bridges in Publication No.FHWA-RD-94-052. 1995, Federal Highway Administration, Mclean, VA: Office of Engineering and Highway Operations R&D.

[71] Tothong, P. and N. Luco, Probabilistic seismic demand analysis using advanced ground motion intensity measures. Earthquake Engineering & Structural Dynamics, 2007. **36**(13): p. 1837-1860. doi: 10.1002/eqe.696.

[72] Buratti, N., Tavano, M., Dynamic buckling and seismic fragility of anchored steel tanks by the added mass method. Earthquake Engng Struct. Dyn., 2014. **43**(1): p. 1-21. doi: 10.1002/eqe.2326.

[73]   Mosleh, A., M. Razzaghi, J. Jara, H. Varum., Development of fragility curves for RC bridges subjected to reverse and strike-slip seismic sources. Earthquakes and Structures, 2016. **11**(3): p. 517-538.doi: https://hdl.handle.net/10216/108695.

[74]   FEMA, HAZUS-MH MR1: Technical Manual. 2003: Federal Emergency Management Agency, Washington DC.

[75]   Karim, K.R., Yamazaki, F., A simplified method of constructing fragility curves for highway bridges. Earthquake Engineering and Structural Dynamics, 2003. **32**(10): p. 1603–1626. doi: 10.1002/eqe.291.

[76]   Elnashai, A., Borzi, B., Vlachos, S., Deformation-based vulnerability functions for RC bridges. Structural Engineering and Mechanics, 2004. **17**(2): p. 215–244.

[77]   Nielson, B.G., DesRoches, R., Seismic fragility methodology for highway bridges using a component level approach. Earthquake Engineering and Structural Dynamics, 2007b. **36**(6): p. 823-839. doi: 10.1002/eqe.655.

[78]   O'Rourke, M.J. and P. So, Seismic fragility curves for on- grade steel tanks. Earthquake spectra, 2000. **16**(4): p. 801-815. doi: 10.1193/1.1586140.